Fermi-surface selective determination of the *g*-factor anisotropy in URu_2Si_2

Gaël Bastien,[1,*] Dai Aoki,[1,2] Gérard Lapertot,[1] Jean-Pascal Brison,[1] Jacques Flouquet,[1] and Georg Knebel[1,†]
[1]*Université Grenoble Alpes, CEA, IRIG-PHELIQS, F-38000 Grenoble, France*
[2]*IMR, Tohoku University, Oarai, Ibaraki 311-1313, Japan*

(Received 8 June 2018; revised manuscript received 19 March 2019; published 24 April 2019)

The *g*-factor anisotropy of the heavy quasiparticles in the hidden order state of URu_2Si_2 has been determined from the superconducting upper critical field and microscopically from Shubnikov–de Haas (SdH) oscillations. We present a detailed analysis of the *g* factor for the α, β, and γ Fermi-surface pockets. Our results suggest a strong *g*-factor anisotropy between the *c* axis and the basal plane for all observed Fermi-surface pockets. The observed anisotropy of the *g* factor from the quantum oscillations is in good agreement with the anisotropy of the superconducting upper critical field at low temperatures, which is strongly limited by the paramagnetic pair breaking along the easy magnetization axis *c*. However, the anisotropy of the initial slope of the upper critical field near T_c cannot be explained by the anisotropy of the effective masses and Fermi velocities derived from quantum oscillations.

DOI: 10.1103/PhysRevB.99.165138

I. INTRODUCTION

The "hidden order" state in the heavy-fermion compound URu_2Si_2 that develops below $T_0 = 17.5$ K is still under debate despite several decades of research [1]. Intense experimental effort has been employed, but right now no spectroscopic probe could unambiguously identify the order parameter. A wide variety of order parameter scenarios have been proposed, most of them based on higher multipolar ordering, various kinds of density wave ordering, or hybridization of the $5f$ states with the conduction electrons as order parameter itself. Recent reviews on the theoretical and experimental status are given in Refs. [2–4]. Interesting proposals are a chirality-density wave ground state of hexadecapoles [5] and odd-parity electric dotriacontapolar order [6].

In addition to the hidden order state, an unconventional superconducting state is formed below $T_{sc} = 1.5$ K, which coexists with the hidden order. This superconducting state is characterized by spin singlet pairing [7]. Recent thermal conductivity and specific heat measurements support a chiral d-wave superconducting gap structure characterized by horizontal line nodes and point nodes at the poles [8,9]. The spontaneous breaking of time-reversal symmetry is in accordance with the experimentally detected chiral d-wave state [10–13].

Like in many heavy-fermion systems, the magnetic susceptibility in URu_2Si_2 at high temperatures shows a Curie-Weiss behavior, indicating a local moment behavior. Below 70 K, hybridization between the $5f$ states and the spd electrons of the ligands sets in, and heavy quasiparticle bands are formed [14,15]. At low temperatures, in the heavy-fermion state, the static bulk susceptibility as well as the dynamical spin susceptibility show a large anisotropy between the *c* axis and the *a* axis of the tetragonal crystal [1,16–18]. Magnetic excitations detected by neutron scattering are strictly longitudinal, indicating Ising-type magnetic fluctuations in URu_2Si_2 [19,20]. Measurements of the nonlinear magnetic susceptibility confirm this Ising character of the magnetic response [21].

The strong Ising character of the $5f$ electrons in URu_2Si_2 has been also confirmed on the basis of density functional theory (DFT) electronic structure calculations [22]. The Ising anisotropy arises from a combination of the peculiar Fermi surface nesting and strong spin-orbit interaction. While in these electronic structure calculations the $5f$ electrons are treated as fully itinerant, other models supposing a localized $5f^2$ non-Kramers doublet ground state could explain the large magnetic uniaxial anisotropy as well [23,24]. In the localized picture, the Ising character of the localized f states of the uranium ions is transferred by hybridization to the heavy quasiparticles, forming a Fermi surface. However, the magnetic and crystal electric field ground-state wave function in URu_2Si_2 is still under discussion [25] and even the localized or itinerant character of the $5f$ electrons.

In the present article, we study in detail the *g*-factor anisotropy for three different Fermi surface pockets in this tetragonal system. The orientation of the sample was tuned to study field directions between [001] and [100] and between [001] and [110], as well as within the basal plane for the quantum oscillation and the upper critical field measurements, so we could determine the *g*-factor anisotropy for different Fermi surface pockets in this multiband system. We compare the Fermi-surface selective *g* factor from the quantum oscillations to the effective *g* factor determined from the anisotropy of the upper critical field.

The *g* factors determined for each Fermi surface show an anisotropy between the *c* axis and the basal plane. In addition, we show that the observed *g* factor of branch β is field dependent. The analysis of the spin-slitting zero of the α branch

*Present address: Leibniz-Institute for Solid State Research (IFW) Dresden, Helmholtzstrasse 20, 01069 Dresden, Germany.
†georg.knebel@cea.fr

is more delicate, as we observe 17 spin-splitting zeros in the (010) plane and only 12 zeros in the (110) plane. This implies either a nonmonotonously varying g factor in the (010) plane or the observation of spin-splitting zeros in the basal plane, which could not be resolved in the present experiment. Our results strongly suggest that the Fermi-surface pockets with strongly anisotropic g factor determine the superconducting upper critical field at low temperature. The superconducting pairing is known (from the large specific heat jump or the high orbital limitation) to be dominantly governed by the heaviest quasiparticle pockets with strongly anisotropic Fermi velocities. In the present state of band-structure calculations in heavy-fermion compounds, there is no derivation of the g factor right at the Fermi level or of its link with the bulk Pauli susceptibility. The interest of this study is to give an experimental framework for future theoretical developments.

A. Fermi surface of URu_2Si_2

The Fermi surface of URu_2Si_2 has been previously studied in detail by magnetic quantum oscillations [26–32], cyclotron resonance measurements [33,34], and angular resolved photoemission spectroscopy (ARPES) [35–42]. According to these experiments and to their comparison with band-structure calculations [43–45], four different Fermi surface sheets have been observed. At the center of the simple tetragonal Brillouin zone, a rather isotropic large-hole Fermi surface α exists. The electron Fermi surface β is four-folded and located between the Γ and X points of the simple tetragonal Brillouin zone. A small elliptical electron Fermi surface γ and a heavy Fermi surface η are located either at the M point or at the Γ point. As URu_2Si_2 is a compensated metal, we can conclude that the quantum oscillation experiments failed up to now to detect a heavy electron pocket which, following band-structure calculations [43,45], is located at the M point of the Brillouin zone. A four-armed cagelike Fermi surface around the α pocket is expected in Ref. [45], while it disappears completely in other calculations [43]. No orbit corresponding to this cagelike structure has been detected in quantum oscillation experiments. Thus, the Fermi surface of URu_2Si_2 has not been completely determined and it is not fully understood.

B. Detection of the g factor

The Ising-type characteristics of the quasiparticles forming the Fermi surface in URu_2Si_2 have been supported from the analysis [46] of old quantum oscillation experiments [27]. This has been inferred from the observation of so-called spin-splitting zeros in the amplitude of the quantum oscillations. In general, the spin splitting of the Fermi surface under a magnetic field gives rise to interference of quantum oscillations from spin-up and spin-down electrons, leading to a modulation of the amplitude of the quantum oscillations. The angular dependence of the amplitude of the first harmonic is given by the spin-damping factor

$$a(\theta) = a_0(\theta)|\cos[\pi g(\theta)m^\star(\theta)/2m_0]|, \tag{1}$$

when the quantum oscillation frequencies and effective masses $m^\star$ for the spin-up and spin-down electrons are equal. The prefactor $a_0(\theta)$ contains the other factors of the Lifshitz-Kosevich formula and is expected to vary slowly with angle [47]. The amplitude of the quantum oscillations vanishes when the product of the g factor and the enhancement factor of the effective mass ($m^\star/m_0$) is an odd integer. This phenomenon is called a spin-splitting zero. It allows for the determination of the product $m^\star g$. The effective mass $m^\star$ can be determined independently from the temperature dependence of the oscillation amplitude. Spin-splitting zeros in quantum oscillations were observed in many systems such as copper or gold and have been used to determine the angular dependence of the g factor in simple metals (see, e.g., Ref. [48]). It is also reported for quasi-two-dimensional metals with strongly anisotropic effective masses [49,50] or in high-T_c superconductors [51]. However, in the case of heavy-fermion and related intermetallic compounds, the observation of successive spin-splitting zeros is rather rare and has been reported only in $CeIn_3$ [52], where the effective mass of the d branch is anisotropic in spite of a cubic system, and in URu_2Si_2.

In URu_2Si_2, the observation of the spin-splitting zero has been reported only for the α branch in the (010) plane [27]. For this branch, the effective mass varies from $m^\star \approx 12m_0$ for field along the c axis to $m^\star \approx 10m_0$ along the a axis; thus, it is rather isotropic [27,29,31]. The observation of the spin-splitting zero for branch α in URu_2Si_2 has been interpreted as signature of an Ising-type g factor with $g^{[001]} = 2.5$ along the c axis and a vanishing small value $g^{[100]} \approx 0$ along the a axis [46].

The g factor determined from quantum oscillations is always an averaged g factor

$$g = \frac{\oint g(\mathbf{k}, \mathbf{B}) v_{\mathbf{k}}^{-1} dk}{\oint v_{\mathbf{k}}^{-1} dk} \tag{2}$$

over the orbit perpendicular to the applied magnetic field [48]. As it depends on $\mathbf{k}$ and the magnetic field direction, $\mathbf{B}$ is a tensor quantity.[1] It is Fermi-surface selective, and its relation to macroscopic properties like the spin susceptibility is not at all straightforward, especially when there is duality between the localized and itinerant character of the $5f$ electrons. To calculate the spin susceptibility, one should determine the g factor for every k point on all the Fermi surface pockets and average over them. As quantum oscillations are only observed on extreme orbits, it seems only possible for almost spherical closed Fermi surfaces and when the complete Fermi surface can be observed in the experiment. In heavy-fermion systems, this is rare.

In a superconductor, the g-factor anisotropy can be determined from the paramagnetic limitation of the superconducting upper critical field H_{c2}. In URu_2Si_2, H_{c2} varies from 3 T along the c axis to 12 T in the basal plane [46,53]. Along the c axis at low temperatures, H_{c2} is determined by the paramagnetic limiting field $\mu_0 H_{c2}^P = \frac{\sqrt{2}\Delta}{\mu_B g}$, which is given by the superconducting gap Δ and the effective g factor for a single-band isotropic superconductor [54]. From the angular dependence of H_{c2} at 30 mK between the c axis

[1] We will use the notation $g^{[100]}$ or g_a for the component of g parallel to the field applied along the a axis, $H \parallel [100]$.

and the basal plane, taking only the paramagnetic limit into account, a strongly anisotropic g factor has been determined with $g^{[001]} = 2.65$ along the c axis and $g^{[100]} \approx 0.5$ for $H \parallel a$ [46]. Lower g-factor values were obtained by fitting the temperature dependence of the upper critical field along the c and a axis taking into account the orbital limit: $g^{[001]} = 1.9$ and $g^{[100]} = 0.2$ [53]. Thus, H_{c2} along the a axis is close to the pure orbital limit. The g factor determined from the superconducting critical field gives, in difference to that from quantum oscillations, an average of all electrons participating in the superconducting pairing. It is only for a single-band isotropic superconductor that it is directly related to the spin susceptibility $\chi/\chi_0 \propto gm^\star/(2m_0)$, where χ_0 and m_0 are the spin susceptibility and band mass of a free electron gas [48].

Previously, spin-splitting zeros have been observed only for the α Fermi surface pocket in URu_2Si_2 at many field angles in the (010) plane [27]. An analysis of the effective g factor from these data has been reported by Altarawneh *et al.* in Ref. [46] and its anisotropy agrees remarkably well with that found from the Pauli limit of the superconducting upper critical field. However, in this previous work, only the spin-splitting zeros of the α pocket in the (010) plane has been taken into account. Here we report the observation of the spin-splitting zero for all observed Fermi surface pockets and extend previous work also to the (110) plane.

II. EXPERIMENTAL DETAILS

URu_2Si_2 crystallizes in the body-centered tetragonal $ThCr_2Si_2$-type crystal structure with space group $I4/mmm$. In the hidden order phase, the symmetry is lowered and the simple tetragonal unit cell volume below 17.5 K is twice that of the paramagnetic state. The space group of the hidden order state is still under discussion as it depends on the symmetry of the hidden order state [55,56]. Three different URu_2Si_2 single crystals (S1, S2, and S3) were used in this study. Samples S1 and S2 have been grown and investigated at CEA Grenoble; S3 has been grown and measured at IMR Oarai. The sample S1 was cut by spark erosion from a large single crystal which has been grown by the Czochralski pulling method in a tetra-arc furnace under argon atmosphere [57]. The samples S2 and S3 were grown by the indium flux method [58]. The residual resistivity ratio $RRR = R(300\,\mathrm{K})/R(0\,\mathrm{K})$ of S1, S2, and S3 are 275, 350, and 300, respectively. Resistance measurements were performed with an electrical current along the [010] direction in top-loading dilution refrigerators from Oxford Instruments down to $T = 22$ mK with maximal magnetic field of 15 T, at CEA Grenoble (S1 and S2) and at IMR Oarai (S3). Because of their irregular geometry, we do not calculate the resistivity and present only the measured resistance for samples S1 and S2. The samples were rotated with respect to the magnetic field using a commercial Swedish rotator which is driven by a stepper motor. The magnetoresistance was measured in S1 and S2 under magnetic fields applied from [001] to [100] and the magnetoresistance of the sample S1 was also measured between [001] and [110] in angular steps of 0.9 deg. The sample S3 has been measured in the angular range from [100] to [110]. In all cases, the electrical current is applied along the [010] direction.

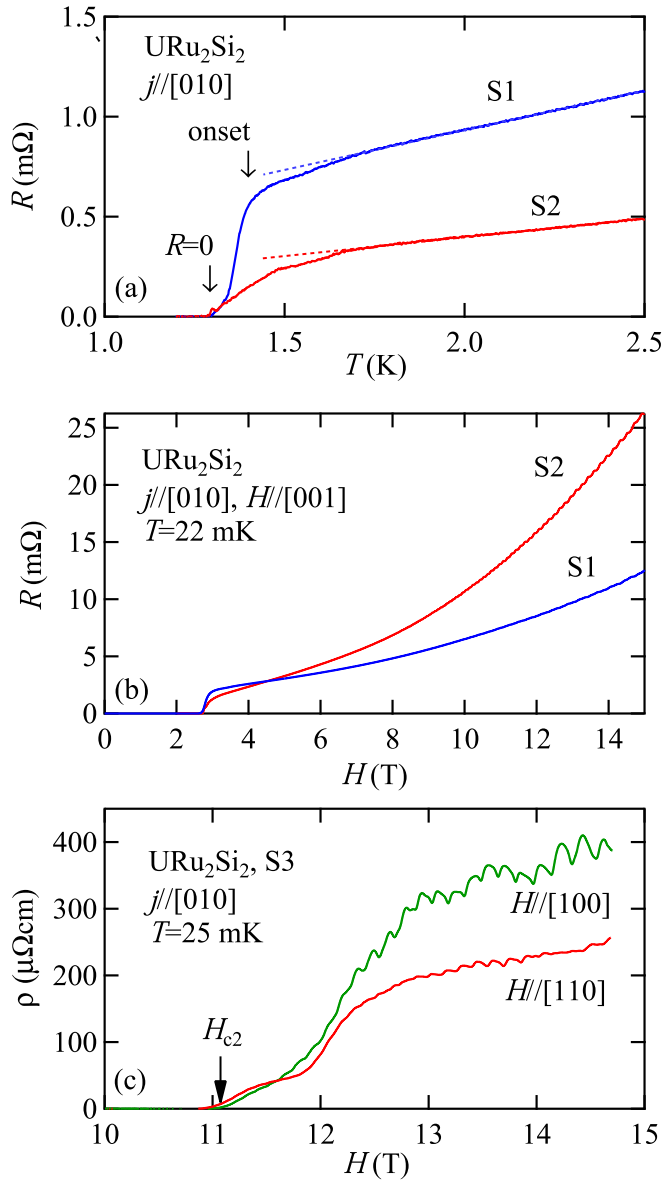

FIG. 1. (a) Temperature dependence of the electrical resistivity of samples S1 and S2. (b) Magnetoresistance at 22 mK for field applied along [001] of S1 and S2. (c) Magnetoresistance of S3 for field along [100] and [110] at 25 mK. The arrow indicates H_{c2} for field along [100].

III. RESULTS

A. Sample characterization

The temperature dependence of the resistance of the two crystals studied in Grenoble is shown in Fig. 1(a). Both samples show zero resistance below $T_c = 1.3$ K. The superconducting onset of S1 is at $T \approx 1.4$ K, while sample S2 shows another pronounced kink at $T = 1.5$ K. As indicated, in both samples, a tiny kink in $\rho(T)$ appears at $T = 1.7$ K indicating incipient superconducting fluctuations. In an extended temperature range from 1.7 to 4 K, the resistance can be parameterized with a power law and we find exponents $n = 1.2$ for S1 and $n = 1.7$ for S2. Such a large variability of the temperature dependence of the resistivity above the

superconducting transition has been reported previously [59], and it indicates the very strong sample dependence of the inelastic scattering in URu_2Si_2. The width of the superconducting transition of S1 defined as $\Delta T_{sc} = T_{sc}^{onset} - T_{sc}^{R=0} \approx 0.1$ K is comparable with previously studied high-quality single crystals [59,60].

The magnetoresistance of the samples S1 and S2 is shown in Fig. 1(b) for a field applied along the c axis. The flux-grown sample S2 shows a stronger magnetoresistance and the amplitude of the Shubnikov–de Haas (SdH) oscillations is larger for this sample, indicating a higher average mean free path. Sample S1 was chosen for the study of the upper critical field H_{c2} at different angles due to the sharper superconducting transition. S2 shows already strong superconducting fluctuations above the transition, and the superconducting transition itself is also broader. In Oarai, we measured the angular dependence of the SdH oscillations in S3 in the basal plane, fine turning the field from [100] to [110] in the field range from 10 to 14.7 T. Figure 1(c) shows the magnetoresistance of this sample for magnetic fields applied along [100] and [110]. Special attention has been taken to avoid a misorientation toward the c axis, which nevertheless cannot be fully excluded. This sample shows extremely large quantum oscillations for $H \parallel [100]$. The observed oscillations amplitude decreases when the field is applied along [110], mainly due to the fact that the current and field directions are 45 deg to each other and the magnetoresistance is between the transverse and longitudinal configuration for $H \parallel [110]$. In both directions, we observe a distinct nonzero resistance between 11 to 12 T. Zero resistance is observed below 11.05 T for $H \parallel [100]$ and 10.95 for $H \parallel [110]$, indicating that H_{c2} is almost isotropic in the basal plane. These values of the upper critical field H_{c2} are lower than those previously reported [27,53,61]. Because of the strong quantum oscillations, it is impossible to determine the width of the superconducting transition from field sweeps.

Figures 2(a) and 2(b) show the fast Fourier transformations (FFT) of the SdH oscillations at 22 mK for a field interval from 9 to 15 T applied along the c axis for samples S1 and S2. The spectra show four fundamental quantum oscillation frequencies, in agreement with previous reports [27–29,31]. For the α branch of sample S2, one could detect up to the third harmonic in this field range. The relative amplitude of the different FFT frequencies changes between samples S1 and S2. While the β frequency has the highest amplitude for S1, the α frequency dominates the spectrum of S2. Figure 2(c) presents the FFT spectrum of oscillations observed in S3 for field applied along [100] in the field range from 12 to 14.7 T. Up to four harmonics of the α branch are observed in this restricted field interval. The previously reported splitting of the α branch in the basal plane [27,31] could not be resolved in this small field interval but the asymmetry of the FFT peak for the α frequency is an indication that the peak is a sum of different frequencies.

B. Upper critical field

Figure 3(a) displays the magnetoresistance at 25 mK for different angles measured on S1. To determine the upper critical field H_{c2}, the criterion $R = 0$ has been chosen. The

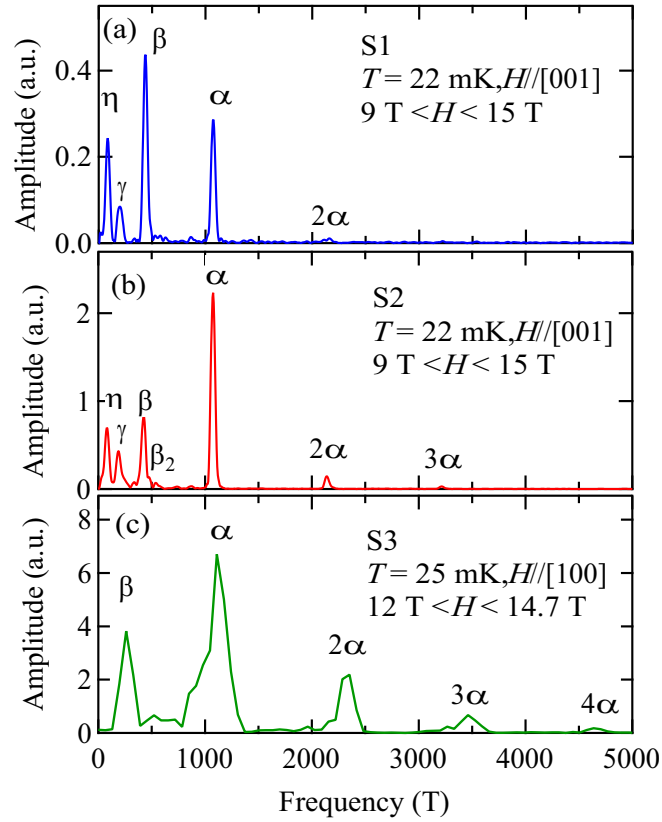

FIG. 2. [(a), (b)] FFT spectra of the SdH oscillations at 22 mK in the field range from 9 to 15 T along the [001] direction for S1 and S2. The quantum oscillation frequencies are indicated. β_2 corresponds to the spin-split Fermi surface of the β branch, which appears due to the nonlinear Zeeman splitting (see text). (c) FFT spectra for S3 at 25 mK in the field range from 12 to 14.7 T applied along [100]. Up to four harmonics of the α branch are observed. The splitting of the α branch could not be resolved in this small field interval.

width of the transition is slightly increasing when the field is turned toward the basal plane. Close to [100], the onset of the superconducting state is no more clearly defined due to the oscillations of the magnetoresistance. Similar to S3, the anisotropy of H_{c2} in the basal plane is very small. We find $H_{c2} = 12.05$ T for $H \parallel [100]$ and 11.95 for $H \parallel [110]$ at 25 mK. Figure 3(b) shows $H_{c2}(T)$ as a function of temperature for different magnetic field directions between [001] and [100]. The temperature dependence of H_{c2} for [001] and [100] is in good agreement with previous studies [27,53]. A thermal conductivity study in URu_2Si_2 showed that the bulk upper critical field would be slightly higher than the resistive one [61]. This small difference between the resistive and the bulk upper critical field will be neglected in the discussion. The angular dependence of the initial slope $-dH_{c2}/dT$ at $T = T_{sc}$, as well as that of H_{c2} at 25 mK, are represented in Fig. 3(c). Both are very anisotropic. The initial slope varies from 5.1 to 11.3 T/K and the upper critical field from $H_{c2} = 2.75$ T to 12.05 T at 25 mK, for fields along [001] and [100] respectively. The initial slope of H_{c2} at T_{sc} allows an estimate of the averaged anisotropy of the Fermi velocity ($H'_{c2} \propto \frac{T_{sc}}{v_F^2}$), which is given by $(v_F^{[001]}/v_F^{[100]})^2 = (\frac{dH_{c2}^{[001]}}{dT}/\frac{dH_{c2}^{[100]}}{dT})^{-1} = 1.5$.

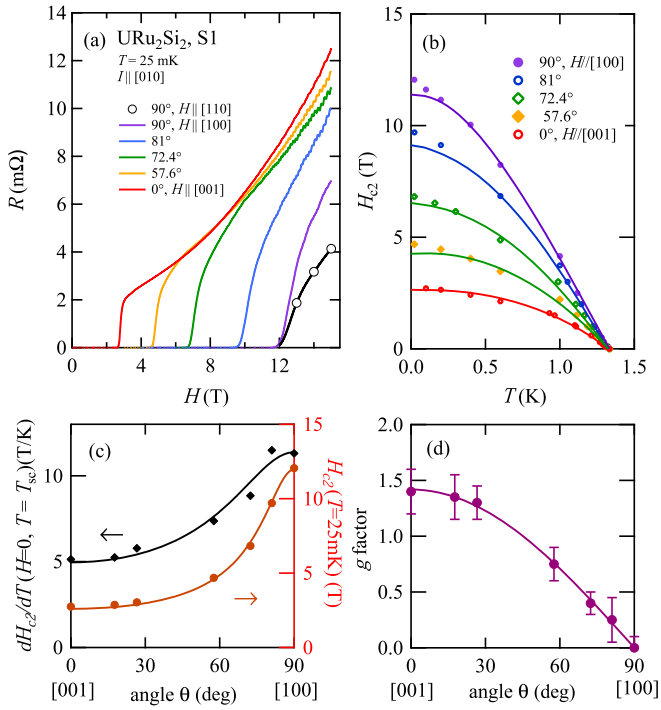

FIG. 3. (a) Magnetoresistance at $T = 25$ mK for sample S1 for different field directions. (b) Temperature dependence of the upper critical field H_{c2} determined by the criterion $R = 0$. The solid lines are fits from the WHH model [62]. (c) Angular dependence of the initial slope $-dH_{c2}/dT(T = T_{sc})$ and the low temperature value $H_{c2}(T = 25\,\text{mK})$ of the H_{c2}. Solid lines are guides to the eye. (d) Angular dependence of the g factor deduced from the fits of the temperature dependence of H_{c2}. The solid line is a fit assuming an uniaxial g-factor anisotropy $g(\theta) = g_c \cos(\theta)$, with $g_c = 1.4$.

Here, $v_F^{[001]}$ and $v_F^{[100]}$ are the average Fermi velocity of the quasiparticles in the plane perpendicular to the direction of the magnetic field along [001] and [100], respectively.

The temperature dependence of H_{c2} has been calculated numerically based on the Werthamer, Helfand, and Hohenberg (WHH) model within the weak coupling and clean limit [62] with even parity pairing.[2] Both the paramagnetic and orbital limits are taken into account and the resulting fits are shown in Fig. 3(b). The orbital limitation is controlled by the average Fermi velocity perpendicular to the applied magnetic field and it determines the initial slope dH_{c2}/dT at T_{sc}, while the paramagnetic limiting field is controlled by the electronic g factor [54]. The WHH calculation reproduces the temperature dependence of H_{c2} reasonably well, except at lowest temperatures, where the values from the experiment are slightly higher than the calculation.

The angular dependence of the g factor extracted from these calculations of H_{c2} is represented in Fig. 3(d). Under a magnetic field along [100], the fit is best for a complete absence of a paramagnetic limitation ($g^{[100]} = 0$). Along [001],

[2]For simplicity, the calculations are performed for an s-wave state. The exact form of the pairing symmetry has only minor corrections to the T dependence.

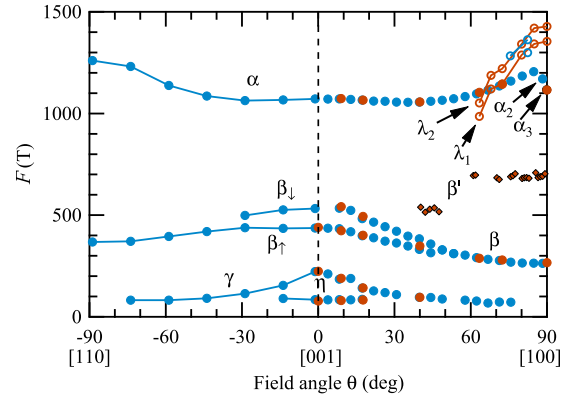

FIG. 4. Angular dependence of the SdH frequencies of URu_2Si_2. Blue and red symbols stand for samples S1 and S2, respectively. The η, γ, β, and α branchs are determined from the fast Fourier transformations (FFT) on the interval 9–15 T. The heavy branch β', which originates from the fourfold pockets of the β Fermi surface, has been determined from an FFT in the field range 12–15 T. The light branches λ_1 and λ_2 have been determined at 600 mK in the field range 9–15 T.

the g factor obtained by the fit is $g^{[001]} = 1.4$. These results are in relatively good agreement with a previous similar study, which yielded $g^{[100]} = 0.2$ and $g^{[001]} = 1.9$ [53]. The angular dependence of the g factor in Fig. 3(c) can be well fitted with $g(\theta) = g^{[001]} \cos(\theta)$, which corresponds to an Ising behavior of the quasiparticles. It is also consistent with the expected angular dependence of the paramagnetic limitation, when $g^{[100]} = 0$ (see Appendix of Ref. [53]). Thus, from the upper critical field measurement, we can conclude that both the initial slope (and thus the Fermi velocity of the quasiparticles) and the average g factor of the dominant band for superconductivity are anisotropic.[3] Essentially, the g factor in the basal plane determined from the superconducting upper critical field is close to zero and it is strongly increasing for fields close to the c axis. The initial slope at T_c (and thus the effective mass) is larger for field in the basal plane than for field along the c axis. Importantly, the anisotropy of the effective mass from the initial slope is opposite to that determined from the quantum oscillation, where the cyclotron masses for magnetic field applied along the c axis is, for all orbits, larger than for field applied in the basal plane [27,29,31]. Thus, the anisotropy of the initial slope cannot be explained by the effective mass model with a single Fermi surface sheet [64]. This point will be discussed in Sec. IV D.

C. Quantum oscillations

The angular dependence of the quantum oscillation frequencies determined at 22 mK is plotted in Fig. 4. All

[3]Another interpretation of the anisotropy of the upper critical field in URu_2Si_2 is based on the field dependence of the pairing interaction [63]. However, it needs a very low value of the coupling constant $\lambda = 0.05$. This value would imply a difference of several orders of magnitude between the characteristic temperature of fluctuations responsible for superconductivity and the superconducting temperature, which seems unrealistic.

previously reported branches have been observed [26–29,31,32], except the light pocket ε, which has been only reported in Ref. [28] to appear above 17 T. The nearly spherical Fermi surface pocket α and the β Fermi surface are in good agreement with previous studies. Close to [100] the α branch splits into at least three different branches in the basal plane [27,31]. The origin of the splitting is not fully understood; one proposal is that it is due to a magnetic breakdown of a very tiny hourglass Fermi surface at the Z point of the Brillouin zone [34]. As shown in Ref. [31], the splitting is very sensitive to the perfect orientation in the basal plane. Under a small angle of 3 deg from the basal plane, it is fully suppressed. As already mentioned, this splitting is not resolved in this experiment as the highest field in our experiment here is only 15 T, but it is compatible with the broad asymetric FFT of sample S3 [see Fig. 2(c)]. Thus, the analysis of the oscillation in the basal plane may not allow for a definitive conclusion.

The β Fermi surface consists of four pockets. As function of angle from [001] to [100], it splits into two branches: the β branch and the heavy branch β' [29]. The appearance of two frequencies β and β' for $H \parallel [100]$ proves that the pockets are located between the Γ and X points of the simple tetragonal Brillouin zone. Furthermore, the β Fermi surface depends strongly on magnetic field [31]. In agreement with the previous report, we can resolve clearly a splitting for the β branch in two frequencies $\beta_\uparrow$ and $\beta_\downarrow$ in the angular range from [001] to 40° toward [110], and from [001] to 15° toward [100], for $H > 8$ T. (The assignments of the spin-up and spin-down branches will be justified below.) In this angle interval, the amplitude of the lower frequency $\beta_\uparrow$ is much stronger than that of $\beta_\downarrow$ and the amplitude of the FFT spectrum is only weakly modulated with angle. However, interferences between the signals from $\beta_\uparrow$ and $\beta_\downarrow$ can be observed on approaching [110] or [100]. It proves, in agreement with the field dependence, that the splitting of the β branch near [001] is a spin splitting. The strong field dependence confirms a nonlinear Zeeman splitting.

The angular dependence of the γ and η branches is similar to the previous report [29]. We want to stress that the cross section of the γ orbit appears larger for a field along the c axis and decreases in size to the basal plane. In contrast, all band-structure calculations [43–45] suggest an elliptical Fermi surface elongated along the c axis.

In addition, we have been able to determine the angular dependence of two light branches λ_1 and λ_2 at temperatures above 600 mK (see Fig. 4), when the amplitude of the heavy branches is strongly suppressed. These branches have been observed in previous experiments in pulsed magnetic fields [32]. From the temperature dependence of the amplitude, which has been measured up to 1 K, we determine the effective masses of these light branches to $m^\star_{\lambda_1} = 1.4 m_0$ and $m^\star_{\lambda_2} = 2.1 m_0$. Band-structure calculations do not predict such light frequencies. They may correspond to the light bands F and G observed in cyclotron resonance experiments [33,34].

The spin degeneracy of the conducting electrons is lifted in an applied magnetic field, leading to an energy difference between the spin-up and spin-down electrons, which is given by the Zeeman term $\Delta E = \frac{1}{2} g \frac{e\hbar}{m^\star} H$. The Fermi surface splits in spin-up and spin-down sheets.

The effect of this spin splitting is equivalent to a phase difference of $\phi = 2\Delta E = \pi g \frac{m^\star}{m_0}$ between the oscillations coming from the spin-up and spin-down electrons and can give rise to interferences, leading to modulations of the amplitude of the quantum oscillations. This simple approach for free electrons neglects all field dependences of the cyclotron orbits, the effective mass, and also the effective spin splitting g factor.

The quantum oscillation frequencies F are related to the extremal cross section $\mathcal{A}$ of the Fermi surface by the Onsager relation $F = (\hbar/2\pi e)\mathcal{A}$. However, the frequency $F_{\rm obs}$, which is measured in the experiment at a finite field, is related to the true quantum oscillation frequency by $F_{\rm obs}(H) = F_{\rm true} - \frac{dF_{\rm true}}{dH}$ [65]. What is measured is the so-called back-projected frequency to zero field. Thus, if the observed frequency is field independent, the true frequency increases linearly with field and thus the Zeeman splitting of the Fermi surface is also linear in field. In the case that the back projection to zero field of the frequencies of the spin-up and spin-down quantum oscillations and the effective masses and mean free path of the quasiparticles do not depend on the spin direction, the angular dependence of the amplitude of the first harmonics of the quantum oscillations can be described by Eq. (1). The amplitude of the quantum oscillations vanishes when the spin-splitting damping factor $\cos(\pi g m^\star/2m_0)$ is zero, i.e., when $g(m^\star/m_0) = 2n - 1$ is an odd integer.

However, if the observed frequency $F_{\rm obs}$ is field dependent, $F_{\rm true}$ has a nonlinear field response. In this case, the observed frequencies $F_\uparrow$ and $F_\downarrow$ of spin-up and spin-down Fermi surfaces are not identical and the damping factor does not vanish. Because of the nonlinear response, the back-projected frequencies for spin-up and spin-down surfaces are not identical and two frequencies are observed. Generally, in heavy fermion systems, the effective mass of the quasiparticles is expected to be spin dependent [66,67] and such a spin dependence has been experimentally observed [68,69].[4] In addition, also the effective g factor can be field dependent. However, the experimental observation of a field-dependent g factor is rare [70].

The magnetoresistance at 22 mK measured in S2 is represented for different field angles from 12.1° to 22.9° from [001] to [100] in Fig. 5. The SdH oscillations from the α branch are clearly resolved. The quantum oscillation amplitude decreases from 12° to nearly 16° and increases for larger angles. A phase shift of 180° can be observed between oscillations observed for angles slightly below and above 16°. This is a clear indication for the appearance of a spin-splitting zero.

Figure 6 shows a contour plot of the amplitude of the FFT spectra calculated in the field interval 12–15 T of the quantum oscillations at $T = 22$ mK as a function of angle for sample S1. The horizontal and vertical axes correspond to the field angle and the oscillation frequency respectively. The solid lines in Fig. 6 gives the angular dependence of the SdH frequencies in this field range. In this color plot, the appearance of splin-splitting zero is clearly observed for the α and β

[4]The detection of spin-splitting zeros excludes the presence of any spontaneous magnetization, as in that case the orbits of spin-up and spin-down electrons have different sizes.

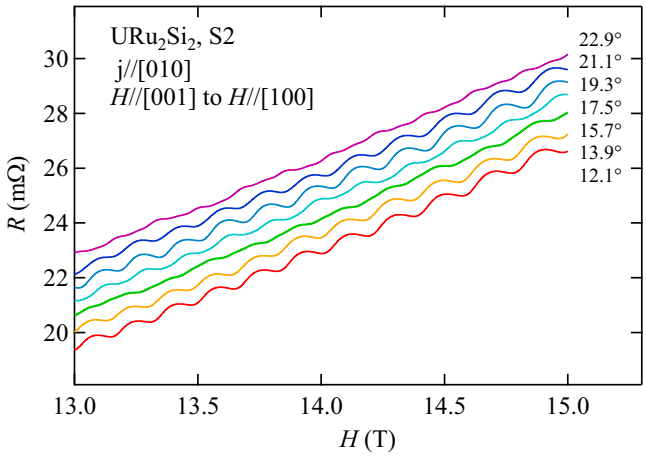

FIG. 5. Resistance measured on S2 for different angles from [001] to [100]. The curves are vertically shifted of 0.5 mΩ for clarity. The amplitude of the SdH oscillations change with increasing angle and is minimal for $\phi = 15.7°$. A phase shift of 180° occurs indicating a spin-splitting zero.

branches. Next we will discuss the oscillation of the amplitude for the different branches in detail.

Figure 7(a) displays the angular dependence of the oscillations amplitude for the α Fermi-surface pocket from [001] to [110] and from [001] to [100] in the field interval 12–15 T measured on S1 (blue circles) and S2 (red crosses). The amplitude is normalized to the value at $H \parallel [001]$. The amplitude oscillates very strongly with the field angle. In the field interval 6–9 T, similar oscillations of the amplitude have been observed which indicates that they are not field dependent. Comparable oscillations of the de Haas–van Alphen (dHvA) amplitude from the α pocket have already been reported in Ref. [27]. While Ohkuni *et al.* observed 16 spin-splitting zeros between [001] and [100], both samples in our measurements show 17 zeros. This difference can be explained by a slight misalignment in the previous experiment [27] around an axis

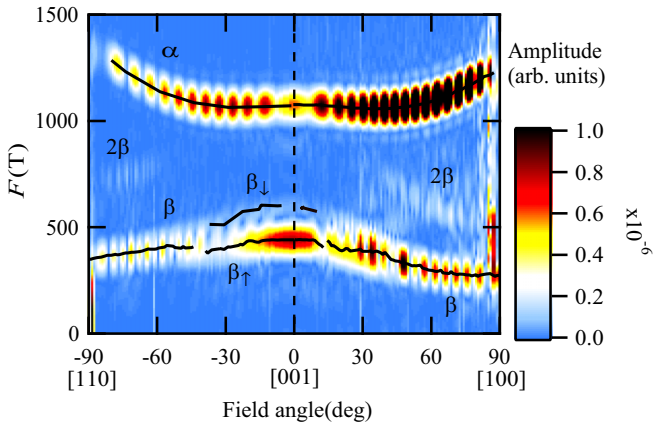

FIG. 6. FFT spectra of quantum oscillations at $T = 22$ mK in the field range from 12 to 15 T as a function of angle for S1. The color code corresponds to the amplitude of the FFT spectra. The solid lines show the angular dependence of α and β frequencies. In the vicinity of [001], the signal of the β branch splits into $\beta_\uparrow$ and $\beta_\downarrow$.

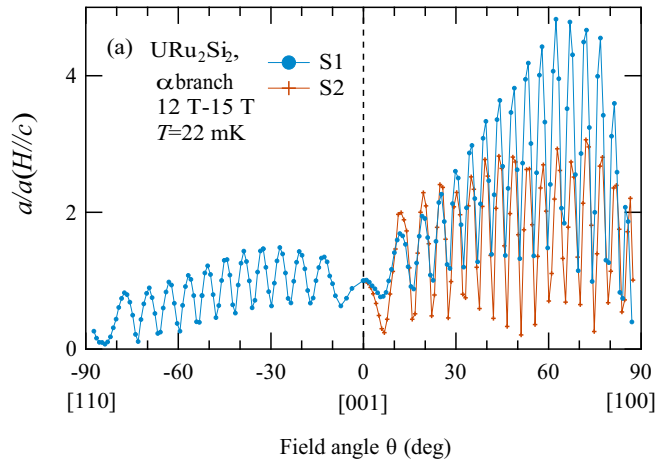

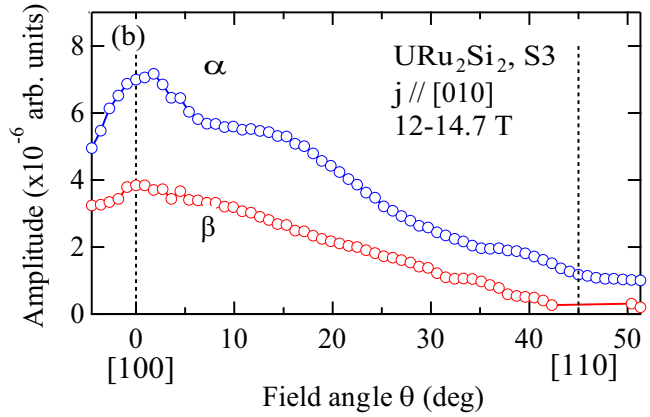

FIG. 7. (a) Renormalized amplitude of quantum oscillations from the α orbit at 22 mK on the field interval 12–15 T as a function of the field direction for S1 and S2. (b) Angular dependence of the amplitudes of the α and β orbits in the basal plane observed in S3.

transverse to the rotation axis. In difference, when turning the field from [001] to [110], we observe only 12 spin-splitting zeros. Note that the amplitude does not vanish completely at the spin-splitting zeros. Already the previous data of Ohkuni *et al.* [27] showed a similar behavior of washed-out spin-splitting zeros. This can be explained by small differences in the frequencies or in the effective masses of spin-up and spin-down bands, which are too small to be resolved in our experiment. Generally, a strong spin dependence of the effective mass is expected in heavy fermion systems [66,71]. In other systems, where spin-splitting zeros have already been reported, such finite values of the amplitude had been reported. In Sr_2RuO_4, it has been argued that the washed-out splin-splitting zeros are due to a different warping for the spin-up and spin-down parts of the cylindrical Fermi surfaces [49]. The variations between different samples may be due to a different amount of impurities. Note that we already observed differences in the relative size of the FFT amplitudes of S1 and S2, which also indicates differences in the Dingle temperature of the various orbits.

As discussed above, in the basal plane the α branch splits in different frequencies [27,31]. Close to [110], three frequencies have been observed with effective masses of $9.7m_0$, $12m_0$, and $17m_0$, which change little as function of angle in the basal

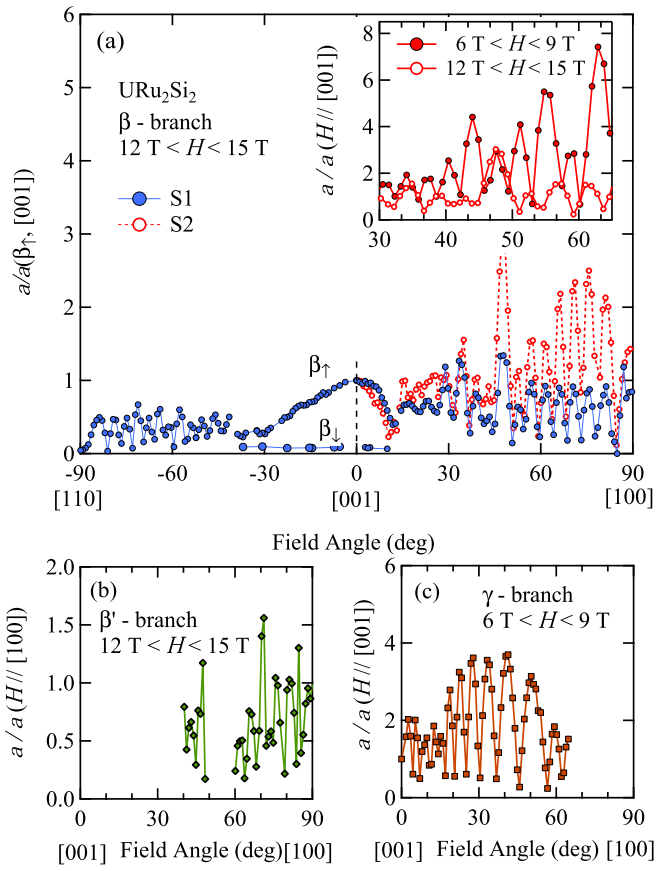

FIG. 8. (a) Normalized amplitude of quantum oscillations from the β branch as function of field angle. In the field range close to [001], spin-zero splitting of the β branch appears and the interference of spin-up and spin-down electrons is no more perfect. In the angular range between [001] to 40° to [110] and to 15° to [100], we clearly observe two frequencies, $\beta_\uparrow$ and $\beta_\downarrow$. The inset shows the angular dependence from 30° to 65° of amplitude of the $\beta_\uparrow$ oscillation in different field ranges for S2. Panels (b) and (c) show the normalized amplitudes of the β' and γ branches measured in S1, respectively. For the γ branch, the field interval has been 6–9 T.

plane. In a limited angular range, Ohkuni *et al.* reported that branch α is even fourfold split [31]. Here, we do not see any splitting of the frequencies in the basal plane, contrary to the angular dependence of the cyclotron resonance frequencies reported in Ref. [33]. In Fig. 7(b), we show the angular dependence of the oscillation frequency observed in the field range from 12 to 14.7 T. As already shown in Fig. 2(c), this splitting is not resolved in the present experiment due to the small field interval from 12 to 14.7 T. Thus, it is not surprising that no spin-splitting zero is observed in the basal plane when turning the magnetic field from [100] to [110]. The decrease of the amplitude from [100] to [110] for both orbits is due to the change of the current direction with respect to the magnetic field from a transverse configuration (current perpendicular to the field) to 45 deg with respect to the field axis. In any case, also in our previous experiment [31] we did not see any indications for any spin-splitting zero.

The angular dependence of the oscillation amplitude from the β branch is represented in Fig. 8(a). It is determined from the FFT spectra in the field range from 12 to 15 T. Near to [001], only very weak oscillations of the amplitude have been observed. This is due to the spin splitting of the β frequency under magnetic field (see Fig. 4 and also Fig. 6 of Ref. [31]). The field dependence of the observed quantum oscillations of branch β can be interpreted as nonlinear field dependence of the minority spin-down Fermi surface, which shrinks with increasing magnetic field and gives rise to a strong increase of the effective mass, as $m^\star = \frac{\hbar^2}{2\pi}\frac{\partial \mathcal{A}(k_H)}{\partial E}|_{E_F}$, where $\mathcal{A}(k_H)$ is the cross-sectional area of the Fermi surface which is perpendicular to the field and k_H is the wave number along the field direction [72]. The effective mass of the spin-minority band increases up to $40m_0$. This nonlinear field dependence of the quantum oscillation frequencies is the consequence of the polarization of the small and heavy electronlike β Fermi-surface pocket under magnetic field along the easy magnetization axis [30–32]. Thermopower measurements in URu_2Si_2 under magnetic field along the c axis show a minimum at $H_m = 11$ T at low temperature [73,74], which also indicates an evolution of the Fermi surface with the magnetic field. Further field-induced Fermi surface changes inside the hidden order state have been detected at higher magnetic field by the Hall effect [28], thermoelectric power [73,74], and quantum oscillations [30–32]. However, all these Fermi surface changes inside the hidden order state have almost no feedback on the measured macroscopic magnetization, which increases almost linearly with field up to $H_c \approx 35$ T, where the hidden order is suppressed, and the magnetization shows a first-order metamagnetic jump [75–77]. Only the NMR Knight shift shows a tiny increase at 23 T [78], where a new quantum oscillation frequency appears [28,31].

In the angular range further away from [001], the spin splitting is no more resolved (see Fig. 4) and the frequencies of spin-up and spin-down Fermi surfaces coincide. While the amplitude of $\beta_\uparrow$ oscillations is maximum at [001], the amplitude of $\beta_\downarrow$ oscillations is much smaller and nearly constant with angle. The amplitude of the β oscillations shows 11 spin-splitting zeros between [110] and 40° from [001] and 13 spin-splitting zeros between [100] and 15° from [001]. Between [001] and [100], both samples show the same number of spin zeros. However, spin-splitting zeros are more clearly resolved in sample S1. In this sample, the amplitude of the β frequency for $H \parallel [001]$ is larger than that of the α branch but, compared to S2, the oscillation amplitude is lower. The oscillation amplitude (in both samples) does not vanish completely at the spin-splitting zeros. Again, it must come from the incomplete cancellation of spin-up and spin-down oscillations due to their amplitude difference and their small frequency and effective mass difference. No spin-splitting zero is observed in the basal plane, when turning the magnetic field from [100] to [110], see Fig. 7(b), but the amplitude decreases smoothly due to the change in the magnetoresistance. The inset in Fig. 8 shows the angular dependence of the oscillations in the field range from 6 to 9 T from 30°–65° from [001] in the (010) plane. Below 9 T, no spin splitting of the β branch is observed. Remarkably, for $6\,\text{T} < H < 9\,\text{T}$, the spin-splitting zeros are closer to each other with eight splin-splitting zeros between 30° and 65° against seven for the field interval 12–15 T. The nonlinear expansion of the spin majority Fermi surface leads to a nonlinear Zeeman effect and to a reduction of the number

of splin-splitting zeros under field. This is different than for branch α, where the same number of spin-splitting zeros had been observed, independent of the magnetic field range.

The amplitude of the β' orbit quantum oscillations is represented as a function of angle between [001] and [100] in Fig. 8(b). It could be determined only in sample S2 in the interval 12–15 T and β' could not be resolved below 40° due to the proximity of its oscillation frequency with $\beta_\uparrow$ and also not between 50° and 60° due to the proximity to the frequency of the second harmonic from β orbit. It shows three spin zeros between 40° and 50° and seven from 60° to 90°.

The γ Fermi-surface pocket is a small ellipsoid with $F_\gamma = 200\,\mathrm{T}$ along [001] and $F_\gamma = 70\,\mathrm{T}$ in plane [31]. Its frequency is too small to be resolved in the interval 12 T–15 T, so this pocket was studied only in the interval 6 T–9 T. The oscillation amplitude in S2 is represented as a function of the angle from [001] toward [100] in Fig. 7(c). Twelve spin-splitting zeros are observed up to 65°. For higher angles, the signal of the γ branch cannot be followed in this field range due to the superconducting transition.

IV. DISCUSSION

A. Analysis of the *g* factor

According to Eq. (1), the amplitude of the quantum oscillations vanishes if $m^\star g/m_0 = 2n - 1$ with n being the number of the spin-splitting zero. The argument of the cos-term of the spin factor $m^\star g/2m_0$ is an integer number at each maximum of the amplitude in the angular dependence. Thus, we can determine the value of $m^\star g/2m_0$ only up to an integer number k. Generally, we can expect the appearance of spin-splitting zeros with field angle, if the g factor or the effective mass are highly anisotropic and g or $(m^\star/m_0)$ are large enough. From the spin-splitting zeros, only the product $g(m^\star/m_0)$ can be determined and the effective mass $m^\star$ has to be determined from the temperature dependence of the oscillations.

For the α Fermi surface, the effective mass $m^\star$ is rather isotropic. We have determined the effective mass $m^\star$ for different directions and find $m^\star_{[001]} = 13.3m_0$, $m^\star_{[100]} = 9.7m_0$, and $m^\star_{[110]} = 11.3m_0$ for fields applied along [001], [100], and [110], respectively. As discussed above, in the basal plane the α branch is split in at least three branches. The effective mass evolves smoothly between these principal axes [see Fig. 9(a)]. Different solutions exist for g and the determination is not unique. Figure 9(b) shows possibilities for the angular dependence of the g factor for the α branch of URu_2Si_2 from the spin-damping factor depending on the choice of k (blue symbols). We assume that the g factor should be largest along [001] and the value $g(m^\star/m_0)$ changes monotonously as a function of field angle, and we choose k as the value of $m^\star g/2m_0$ at the closest amplitude maximum from [100].

For $k = 0$, the data suggest a strong anisotropy of g from [001] to the basal plane varying from $g_\alpha^{[001]} \approx 2.5$ to $g_\alpha^{[100]} \approx 0$ along the a direction. However, as we have only observed 12 spin-splitting zeros when turning the angle from [001] to [110] and the effective mass does not change significantly between [100] and [110], we find $g_\alpha^{[110]} \approx 1.1$ along [110]; i.e., it is not vanishing but would indicate a large anisotropy of g in the basal plane. The main difference between the curves for the different values of k is a vertical shift, so the variation of the effective mass with angle gives only a small correction.

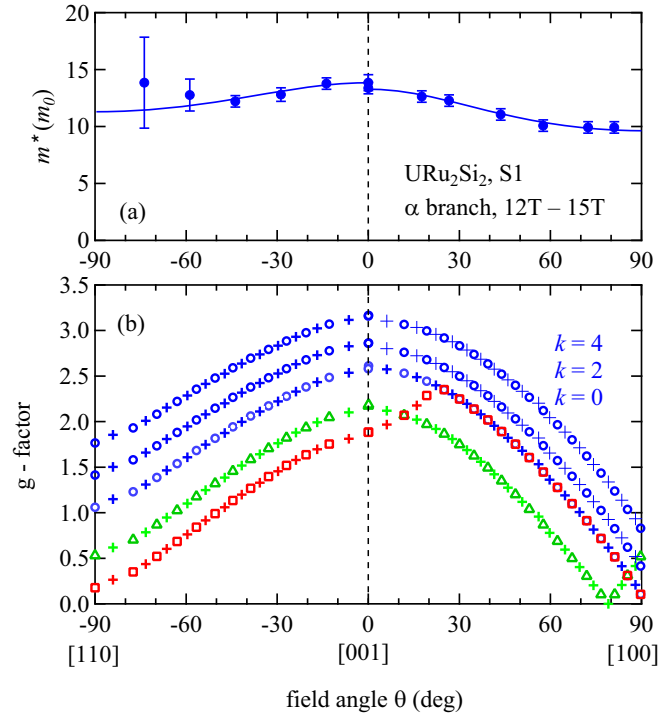

FIG. 9. (a) Angular dependence of the effective mass of the α branch in the field range from 12 T to 15 T. (b) Angular dependence of the g factor for the α branch of URu_2Si_2 for different values from $k = 0$, 2, and 4. Crosses are from the spin-splitting zeros, and circles are from the maxima of the amplitude of the SdH amplitude. The red and green curves give possible scenarios.

Nevertheless, as we observed 17 spin-splitting zeros from [001] to [100], but only 12 from [001] to [110], 5 spin-splitting zeros have to be observed in the basal plane. This is at odds with the variation of the SdH amplitude in the basal plane shown in Fig. 7(b), and also with our previous high field experiment [31] and that of Ohkuni *et al.* [27]. As discussed above, the splitting of branch α could not be observed in our present experiment with maximal field of 15 T. Assuming the three orbits of the α branch (α_1, α_2, and α_3) are spin degenerated, the observed oscillation amplitude would originate from the interference between oscillations of the six orbits. It explains why it is nearly constant with the magnetic field angle between [100] and [110]. In the previous experiment in the field range 12 to 30 T [31], where the splitting of the α branch has been resolved, only for the branch α_2 may a spin-splitting zero occur between [100] and [110]. On the contrary, we have observed 17 in the (010) plane and 12 in the (110) plane, which means that the phases of the oscillations change by 17π and 12π respectively. This suggests the occurrence of five spin-splitting zeros in plane, and the phases of the oscillations change by 5π, under the assumption that $gm^\star$ has a monotonous evolution from the c axis to the basal plane. If we allow a nonmonotonous variation of the g factor, possible solutions could be a maximum (red

curve in Fig. 9) or a minimum of the g factor (green curve).[5] Only if we take into account a nonmonotonous variation of g can a self-consistent solution for the α branch be found from our data.[6]

The cyclotron resonance experiment reported in Ref. [33] showed an unusual splitting of the sharpest observed resonance line which is assigned to the α Fermi surface sheet under in-plane magnetic field rotation from [100] to [110] in the basal plane. The observed splitting is explained by a domain formation which breaks the tetragonal symmetry and accounts for the in-plane mass anisotropy which has heavy (hot) spots only near the orbit for $H \parallel [110]$ and $H \parallel [\bar{1}10]$. This domain formation suggests explaining the observed breaking of the tetragonal symmetry in the basal plane [79]. However, the recent high-resolution x-ray experiment [80–82] and also NMR results [6,83] do not confirm the previously reported tetragonal symmetry breaking [33,34,79,84,85].

The heavy β pocket shows a very strong field dependence above 8 T for $H \parallel [001]$. The observed SdH frequency splits under magnetic field as a consequence of the nonlinear Zeeman effect [31,32]. Therefore, the g factor was calculated in the field interval 6–9 T with reduced effect of the nonlinear field splitting, and for comparison, in a higher field range from 12 to 15 T. In Fig. 10(a), we plot the angular dependence of the mass of the β branch determined for samples S1 and S2. We observe an almost constant effective mass for the β branch within the error bars. Therefore, we use $m^\star \approx 21 m_0$, independent of angle. In difference, our previous data showed that the effective mass of the β branch shows a rather strong angular dependence changing from $m^\star_\beta \approx 23 m_0$ for field along [001] to $m^\star_\beta \approx 13.5 m_0$ [29,31]. This is probably due to the strong field dependence of the effective mass, in particular above 15 T.

The g-factor analysis is performed for the field values and directions, where the splitting of branch β is not resolved. The effective mass used for the analysis was measured and the same field interval and is thus an average mass of spin-up and spin-down electrons. The obtained effective g factor is defined as $g_{\text{eff}} = \frac{1}{\mu_0 \mu_B}(dE_{F_\uparrow}/dH - dE_{F_\downarrow}/dH)$ and is thus an average effective g factor of both spins. The effective g factor may depend of the spin in the vicinity of the c axis as both spin shows different field dependences of the quantum oscillations frequencies.

Figure 10(b) shows the angular dependence of the g factor g_β, in the field interval from 12 to 15 T for angles from [110] to [001] and from [001] to [100]. It depends little on the angular dependence of $m^\star$: An almost similar angular dependence is obtained by taking the angular dependence of the effective mass as obtained in Refs. [29,31] (open circles). Near to [001], we could not determine the g factor from the spin-splitting zeros due to the nonlinear splitting of the β branch with field, and the observation of two different frequencies

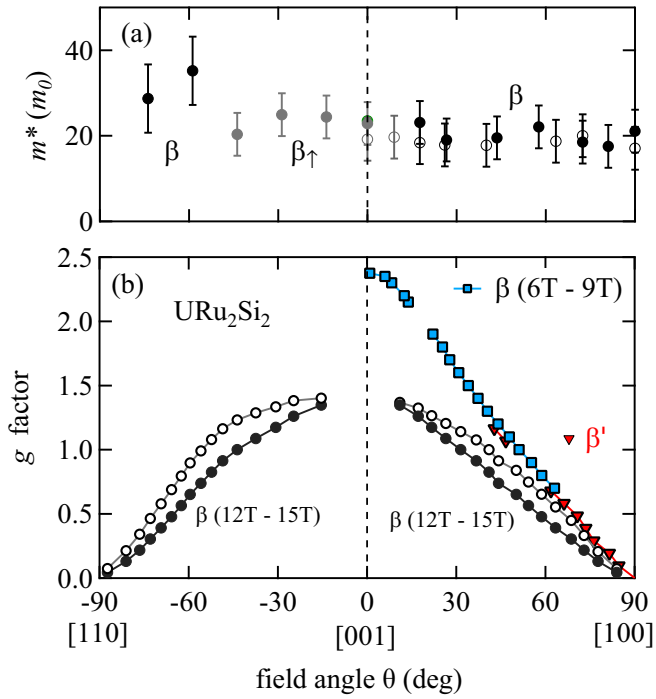

FIG. 10. (a) Angular dependence of the effective mass of the β branch in the field range 12–15 T. Closed (open) circles are for S1 (S2), respectively. Gray symbols mark the effective mass for the spin-split spin-up branch $\beta_\uparrow$. (b) Angular dependence of the g_β factor for the β branch of URu_2Si_2 for the most anisotropic scenario with $k = 0$. Other solutions can be found by shifting the curves upward. Black circles give the g factor in the field range 12–15 T with a constant mass as in determined in the field range from 12 to 15 T [see upper panel (a)]. Open circles give g, assuming the angular dependence of the effective mass in Ref. [31]. Blue squares show the result for the g factor in a lower field range from 6 to 9 T. Red triangles indicate the angular dependence of g for the heavy orbit β' from [001] to [100].

($\beta_\uparrow$ and $\beta_\downarrow$) for $H \parallel [001]$. As discussed above, the number of spin-splitting zeros for the β branch is reduced under magnetic field. This field dependence is a consequence of the polarization of the small and heavy electron Fermi-surface pockets β under magnetic field along the easy magnetization c axis [31,32]. Thus, we plot in Fig. 10 the analysis of the g factor for the β branch also in the field interval $6\,\text{T} < H < 9\,\text{T}$ in the angular range from [001] to [100]. Its extrapolation up to [100] gives a very strong g-factor variation $g_\beta^{[001]} - g_\beta^{[100]} \approx 2.4$. Between [001] and [110], the oscillation could not be detected in the field interval 6–9 T. The variation of the g factor for the β' branch in the field interval 12–15 T with angle from [001] to [100] is also represented in Fig. 10. The effective mass for β' could be measured only under magnetic field along [100], and we found $m^\star_{\beta'} = 20.6\, m_0$. This mass is considered as angle independent, too. The angular variation of the g factor for the β' branch appears identical to that of the β branch, within the error bars.

To analyze the g-factor anisotropy of the γ branch, the strong anisotropy of its effective mass has to be taken into account, as shown in Fig. 11(a). The effective mass decreases strongly with angle from $m^\star_\gamma = 11.5 m_0$ at [001] to $m^\star_\gamma = 4.5 m_0$ at 40° to [100]. If the value of $m^\star g/2m_0$ at the first

[5]Of course, other solutions may be possible too.

[6]These are only valid under the assumption that there is no spin-splitting zero in the basal plane. Nevertheless, there is no other experiment that supports a nonmonotonous variation of a physical property in the (010) plane and thus it is difficult to imagine that g has a maximum near 30 deg from the c axis.

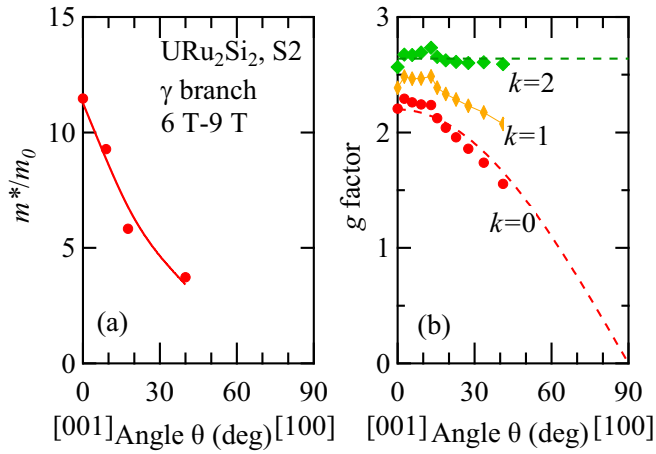

FIG. 11. (a) Angular dependence of the effective mass of the γ branch in the field range 6–9 T. (b) Different possibilities for the angular dependence of the g factor (see text).

detected amplitude maximum from [001] is $k_\gamma = 0$, then the g factor decreases with angle and would reach zero around [100]. The g factor of the γ pocket for this scenario is represented in Fig. 11(b) (red circles). In this case, its angular dependence could be fitted by $g_\gamma(\theta) = g_\gamma([001])\cos(\theta)$ with $g_\gamma([001]) = 2.2$ corresponding to an Ising behavior of the quasiparticles. However, if we choose $k_\gamma = 2$, the occurrence of the spin-splitting zeros can be explained from the anisotropy of the effective mass, and the data can be fitted with a constant g factor $g_\gamma = 2.6$. This shows that the g-factor determination from the quantum oscillations is generally ambiguous.

B. Anisotropy of the *g* factor

By quantum oscillation experiments, we have been able to investigate the conduction electron g factor of URu_2Si_2 selectively for different Fermi-surface pockets. For the α Fermi pocket, our results are compatible with a rather large g-factor ansisotropy. We could show that the angular dependence is not universal between [001] and the basal plane, resulting for the α branch in an unexplained anisotropy in the basal plane. From the present experimental situation, it is not possible to make definite conclusions on the values of the g factor of the α Fermi surface pocket. The set of values $g_\alpha^{[001]} \approx 2.5$, $g_\alpha^{[100]} \approx 0$, $g_\alpha^{[110]} \approx 1$ is only a possible solution, under the assumption of a monotonously varying g factor from the c axis to the basal plane (see Fig. 9). However, this would imply a strong anisotropy in the basal plane, which is not observed here. Furthermore, we also did not observe any anisotropy of the upper critical field in the plane which supports a constant g factor in the basal plane. New high-field experiments in the basal plane in a larger field range than studied here, with perfect orientation with respect to the c axis, may resolve directly the observed anisotropy.

The g factor for the β Fermi-surface pocket is also highly anisotropic. The analysis in the field range from 6 to 9 T suggests that g_β is varying from $g_\beta = 0$ in the plane to $g_\beta = 2.4$ for $H \parallel [001]$. Interestingly, the determination of the g factor seems dependent on the magnetic field. From the analysis of the spin-splitting zeros in the field range from 12 to 15 T, a possible solution is a vanishing g factor in the basal plane and $g_\beta = 1.5$ along the c axis. This field dependence of the measured g factor may be an experimental artifact coming from the field and spin dependence of the effective mass of the β branch, which could not be precisely determined in this study and was neglected in the extraction of the g factor. Under these conditions, the most reliable value for the g factor of the β branch would be the one extracted on the field interval 6–9 T. In this field range, the g-factor variation for the β branch is similar to the variation of g_α and one possible solution for g_γ in the same plane. We point out that even the angular dependence of g for the heavy branch $\beta\prime$ show the same anisotropy. Thus, we can conclude that the g factor of all Fermi surfaces show a strong angular dependence. However, this variation of g is slightly bigger than that determined from the weak coupling analysis of the upper critical field $g^{[001]} - g^{[100]} = 1.5$.

A relativistic DFT calculation predicted an Ising behavior for the bandlike $5f$ electrons in URu_2Si_2 with magnetic moments along the c axis and no anisotropy in the basal plane [22,86]. Here, the $5f$ electrons are treated as fully itinerant and the calculation is performed for the antiferromagnetic phase, which has practically the same Fermi surface than the hidden order state [29,43–45]. This is justified as the Fermi surfaces for the localized $5f^2$ or for the localized $5f^3$ uranium configuration are not in correspondence to the experimentally observed ones [44]. Furthermore, the Fermi surface pockets obtained in the itinerant $5f$ picture are in agreement with all quantum oscillation and ARPES experiments. The Ising anisotropy of the quasiparticles in the DFT calculation is a result of the peculiar Fermi surface nesting at the hidden order transition and of the strong spin-orbit coupling. All uranium $5f$ states have mainly a total angular momentum $j = 5/2$, and in the paramagnetic state each of the Fermi surface pockets important for the nesting at the hidden order transition has a specific $j_z = \pm 5/2$ or $j_z = \pm 3/2$ character with almost no mixing [45,86]. As a result of the doubling of the unit cell [29,36,87] and concomitant gap opening at the hidden order transition [88–90], electronic band-structure calculations show that most of the Fermi surface with $j = \pm 5/2$ character is lost and the α and β pockets have mainly $j_z = \pm 3/2$ components. Only the pockets at the M point have a $j_z = \pm 1/2$ character [45]. If the $j_z = \pm 1/2$ component is dominant, then $g^{[100]}$ or $g^{[110]}$ will be larger than $g^{[001]}$.

A different theoretical approach claims that the Ising quasiparticles in URu_2Si_2 result from the hybridization of the conduction electrons with Ising non-Kramers $5f^2$ doublet states of the uranium atoms [23,91] starting from a localized picture of the $5f$ electrons. However, recent nonresonant inelastic x-ray scattering experiments show that the ground state consists mainly of singlet states in the U^{4+} $5f^2$ configuration [25].

The g tensor has never been determined for any heavy fermion system from electronic band-structure calculations. A main difficulty is knowing the real crystalline electric ground state of the magnetic ions. Furthermore, in URu_2Si_2, heavy bands are formed due to the strong hybridization of the s, p, d states with the $5f$ states. Therefore, the crystalline field levels are broadened and not clearly observed in spectroscopic experiments. In the localized approach for

a U^{4+} ($5f^2$) configuration, the Landé's g_J factor in an intermediate coupling regime is $g_J = 0.824$ and for a U^{3+} ($5f^3$) configuration is $g_J = 0.744$ [92]. First-principles dynamical mean-field calculations concluded that for URu_2Si_2, the $5f^2$ configuration has the dominant weight [14]. The multiplet of the $5f^2$ has a total angular momentum $J = 4$ and splits into five singlets and two doublets. The doublets are linear combinations of the $|J_z = \pm 3\rangle$ and $|J_z = \pm 1\rangle$ [93]. The lowest doublet is $|\uparrow\rangle = \cos\theta|J_z = 3\rangle + \sin\theta|J_z = -1\rangle$ and $|\downarrow\rangle = \cos\theta|J_z = -3\rangle + \sin\theta|J_z = 1\rangle$, with θ being the angle between the c axis and the basal plane. In this case, the g factors are anisotropic and $g_z = g_J(3\cos^2\theta - \sin^2\theta)$ and in the basal plane $g_x = g_y = 0$. However, this g factor in the fully localized picture has never been observed.

This localized approach has been discussed in Ref. [46] and the authors fit the g-factor anisotropy of the α pocket in the angular range from [001] to [100] and got $\cos\theta = 0.8$. As mentioned above, the g factor determined by quantum oscillations is Fermi surface selective, and results from an average of the g factor of electrons on the orbit perpendicular to the applied magnetic field. We have shown that the g factor for all detected Fermi surfaces are consistent with a strong g-factor anisotropy.

C. Comparison to other heavy-fermion system

The determination of the g factor in heavy-fermion systems is rare. A standard method to determine the g factor in magnetic insulators is electron spin resonance (ESR). However, a narrow ESR line in Kondo lattices have been reported only in some Yb- or Ce-based compounds which show very strong ferromagnetic fluctuations such as, e.g., $YbRh_2Si_2$ or CeRuPO [94,95]. Several theories are devoted to explain the linewidth narrowing in these systems starting from a localized or an itinerant model approach [96–98]. In these systems, the large anisotropy of the g factor reflects the local anisotropy in the intersite correlations. In $YbRh_2Si_2$, the anisotropy of the local g_f factor of the Yb ion is about a factor 20, $g_{f\perp} = 3.6$ and $g_{f\parallel} = 0.17$, and reflects the large anisotropy of the susceptibility.

Spin-splitting zeros have been used to determine the angular dependence of the g factor in simple metals such as gold or copper (see, e.g., Refs. [48,99]).[7] Whereas quantum oscillations are studied for almost every heavy-fermion system which could be grown in sufficiently high quality, the observation of spin-splitting zeros and so the determination of the g factor is very rare. Especially in systems showing strong Ising-type anisotropy, it has never been observed. In $CeRu_2Si_2$, the best studied example, it has not been observed, although the Fermi surface has been determined in great detail by quantum oscillation experiments (for a review, see Ref. [100]). This may be due to topology difference of the spin-up and spin-down Fermi surfaces. In URu_2Si_2, only small closed Fermi surface pockets exist in the hidden order state, whereas in $CeRu_2Si_2$ large pockets are detected and also open Fermi surfaces exist.

Spin-splitting zeros have been observed in the cubic $CeIn_3$, which orders antiferromagnetically below 10 K. One of its dHvA branches, named d, which corresponds to a closed spherical Fermi surface centered at the Γ point in the Brillouin zone, has a highly anisotropic cyclotron effective mass. While the effective mass is about $2–3m_0$ for $H \parallel [100]$, it reaches $12–16m_0$ for $H \parallel [110]$. In $CeIn_3$ the determination of the g factor from the spin-splitting zeros of the dHvA oscillations has not been unambiguous, because of the integer k for $g(m^\star/m_0) = 2(n + k) - 1$ [52]. The effective mass is usually isotropic, if the topology of the Fermi surface is spherical in a highly symmetric crystal structure such as a cubic system. In $CeIn_3$, this anisotropic effective mass on the spherical Fermi surface is probably due to the consequence of strong electron correlations with anisotropic $4f$ contribution on the Fermi surface, leading to hot spots at the antiferromagnetic wave vector.

D. Relation between g-factor anisotropy and hidden order and superconductivity

As pointed out in Ref. [101], the strong uniaxial g-factor anisotropy is also compatible with an unconventional commensurate charge density wave. Recently, a chirality-density wave has been proposed as order parameter of the hidden-order state from Raman-scattering experiments, where a particular inelastic excitation with A_{2g} symmetry has been observed [5,87]. The proposed density wave is in agreement with the previously determined folding of the Brillouin zone along the c axis at the hidden order transition and confirms the change from a body-centered-tetragonal to a simple-tetragonal electronic structure. For commensurate antiferromagnetically ordered systems, it appears that due to the anisotropic spin-orbit character of the Zeeman coupling, the transverse component of the g tensor shows a significant momentum dependence: It vanishes in the plane perpendicular to the direction of the staggered magnetization due to a conspiracy of the crystal symmetry with that of the antiferromagnetic order [102–104]. If such a scenario is valid for the hidden order state with a characteristic ordering vector $Q_{HO} = (001)$, the appearance of the spin-splitting zeros would not be due to a local property of the U ion but to a collective ordering in the hidden order state.

This would also explain why almost the same anisotropy of the electronic g factor is observed on the different Fermi-surface pockets. The remaining differences are due to differences in the effective mass and to details in the band structure, which results in a momentum-dependent spin-orbit coupling.

Finally, we want to compare the g-factor anisotropy determined from quantum oscillations with that deduced from the anisotropy of the upper critical field. The g factor determined from the paramagnetic limitation of the upper critical field H_{c2} gives an average over all the Fermi-surface pockets contributing to the superconducting state. Near T_c, the observed initial slope of the upper critical field near T_{sc} for a clean superconductor, $H'_{c2} \propto \frac{T_{sc}}{v_F^2}$, where v_F is an average Fermi velocity perpendicular to the applied field. The Fermi velocities can be determined from the quantum oscillation experiments

[7]While in Cu the g factor is isotrope, a spin-splitting zero appears near 13 deg from [111] due to the anisotropy of the effective mass. In the noble metals like Au, the g factor is anisotropic [48,99].

TABLE I. Fermi velocities $v_F = \frac{\hbar}{m^\star}\sqrt{\frac{2\pi F}{\Phi_0}}$ for different Fermi surface pockets in URu_2Si_2. F and $m^\star$ are the oscillation frequency and the effective mass of the corresponding Fermi surface pocket. $v_F^{[001]}$, $v_F^{[100]}$ (m/s), and $v_F^{[110]}$ (m/s) give the Fermi velocities for field applied H along [001], [100], and [110], respectively.

	$v_F^{[001]}$ (m/s)	$v_F^{[100]}$ (m/s)	$v_F^{[110]}$ (m/s)	
α	16 340	24 062	20 860	(this work)
β	6625	5157	6070	(this work)
γ	10 760	8000	9450	(Ref. [31])
η	4000			(Ref. [29])

and are given in Table I for different Fermi-surface pockets. It is obvious that the strong anisotropic initial slope of the upper critical field cannot be explained by the anisotropy of the observed Fermi velocities. Indeed, to explain the factor 2.2 of anisotropy between H_{c2} for $H \parallel c$ or $H_\perp$, a factor 1.5 is required on the corresponding Fermi velocities. For the β branch, which has the smallest Fermi velocity observed, the values of $v_F \perp H$ are of the right order to explain the measured value of $H_{c2} \approx (-11\,\mathrm{T/K})$, applying formulas for a spherical Fermi surface and s-wave superconductivity ($v_F = 6050\,\mathrm{m/s}$). But then, a value of 8900 m/s would be required for $H \parallel c$, much larger than the actual value. This points out the difficulty of precise quantitative comparisons between measured normal-state properties and H_{c2} measurements: Already for s-wave superconductors, it is known that the average v_F determining H_{c2} involves an average over all Fermi sheets weighted by the pairing potential [105,106]. In the case of the proposed d-wave pairing [8,9], the strong gap anisotropy may play a dominant role in the determination of the orbital anisotropy of H_{c2}. However, numerical calculations are required, as well as a complete determination of the Fermi surface of URu_2Si_2: The heaviest mass—the anisotropic electron Fermi surface centered at the M point of the simple tetragonal Brillouin zone [45]—and so possibly the dominant FS sheets for the control of H_{c2} are still not detected in the quantum oscillations.[8]

A next important step in understanding the Fermi surface and its feedback on the hidden order would be to determine completely the Fermi surface in the high-pressure antiferromagnetic state. It is known from SdH experiments that the quantum oscillation frequencies and the effective masses of the main Fermi-surface branches evolve smoothly from the hidden-order phase at low pressure to the antiferromagnetic state above 1 GPa [29,107]. A detailed study of the angular dependence under high pressure will show whether the observed anisotropy of the g factor is a particular characteristic of the hidden order.

[8]This heavy orbit may be observed by cyclotron resonance experiments [33,34].

V. CONCLUSION

We have determined selectively the electronic g factor and its anisotropy for the α, β, and γ Fermi surface pockets of URu_2Si_2 between [001] and the basal plane. For all detected Fermi surface pockets, our results are consistent with a strongly anisotropic g factor. For the β and γ branches, possible solutions exist with vanishing in plane g factor. For the α branch, we observed different numbers of spin-splitting zeros in the (010) and (110) planes, which indicate either a nonmonotonous variation of the g factor in one of these planes or an additional anisotropy in the basal plane. Future experiments in high magnetic fields have to be performed to clarify the g-factor anisotropy of the α branch. The determined anisotropy of the g factor by quantum oscillations is in good agreement with that from the superconducting upper critical field. However, the anisotropy of the initial slope of the upper critical field cannot be explained simply by the observed Fermi surface pockets. An anisotropic heavy Fermi surface pocket still has not been detected in quantum oscillations. The reported determination of the anisotropy of the g factor by quantum oscillations is an important reference for other heavy-fermion systems, showing that itinerant quasiparticles in a metal can have a very strongly anisotropic g factor (Ising-like). Moreover, we hope that our results will stimulate calculations of the g factor from the electronic band structure.

ACKNOWLEDGMENTS

We thank H. Harima, H. Ikeda, G. Zwicknagl, V. P. Mineev, J. P. Sanchez, H. A. Krug von Nidda, E. Hassinger, A. Pourret, P. Chandra, and P. Oppeneer for valuable and fruitful discussions. Furthermore, we are grateful to H. Harima for critical reading of the manuscript. This work has been supported by ERC (NewHeavyFermion) and KAKENHI (JP15H05882, JP15H05884, JP15K21732, JP16H04006, and JP15H05745).

[1] T. T. M. Palstra, A. A. Menovsky, J. van den Berg, A. J. Dirkmaat, P. H. Kes, G. J. Nieuwenhuys, and J. A. Mydosh, Phys. Rev. Lett. **55**, 2727 (1985).
[2] J. A. Mydosh and P. M. Oppeneer, Rev. Mod. Phys. **83**, 1301 (2011).
[3] J. Mydosh, Philos. Mag. **94**, 3640 (2014).
[4] J. Mydosh and P. Oppeneer, Philos. Mag. **94**, 3642 (2014).
[5] H.-H. Kung, R. E. Baumbach, E. D. Bauer, V. K. Thorsmølle, W.-L. Zhang, K. Haule, J. A. Mydosh, and G. Blumberg, Science **347**, 1339 (2015).
[6] S. Kambe, Y. Tokunaga, H. Sakai, T. Hattori, N. Higa, T. D. Matsuda, Y. Haga, R. E. Walstedt, and H. Harima, Phys. Rev. B **97**, 235142 (2018).
[7] T. Hattori, H. Sakai, Y. Tokunaga, S. Kambe, T. D. Matsuda, and Y. Haga, Phys. Rev. Lett. **120**, 027001 (2018).

[8] Y. Kasahara, T. Iwasawa, H. Shishido, T. Shibauchi, K. Behnia, Y. Haga, T. D. Matsuda, Y. Onuki, M. Sigrist, and Y. Matsuda, Phys. Rev. Lett. **99**, 116402 (2007).

[9] S. Kittaka, Y. Shimizu, T. Sakakibara, Y. Haga, E. Yamamoto, Y. Ōnuki, Y. Tsutsumi, T. Nomoto, H. Ikeda, and K. Machida, J. Phys. Soc. Jpn. **85**, 033704 (2016).

[10] G. Li, Q. Zhang, D. Rhodes, B. Zeng, P. Goswami, R. E. Baumbach, P. H. Tobash, F. Ronning, J. D. Thompson, E. D. Bauer, and L. Balicas, Phys. Rev. B **88**, 134517 (2013).

[11] T. Yamashita, Y. Shimoyama, Y. Haga, T. D. Matsuda, E. Yamamoto, Y. Onuki, H. Sumiyoshi, S. Fujimoto, A. Levchenko, T. Shibauchi, and Y. Matsuda, Nat. Phys. **11**, 17 (2014).

[12] I. Kawasaki, I. Watanabe, A. Hillier, and D. Aoki, J. Phys. Soc. Jpn. **83**, 094720 (2014).

[13] E. R. Schemm, R. E. Baumbach, P. H. Tobash, F. Ronning, E. D. Bauer, and A. Kapitulnik, Phys. Rev. B **91**, 140506(R) (2015).

[14] K. Haule and G. Kotliar, Nat. Phys. **5**, 796 (2009).

[15] N. Bachar, D. Stricker, S. Muleady, K. Wang, J. A. Mydosh, Y. K. Huang, and D. van der Marel, Phys. Rev. B **94**, 235101 (2016).

[16] Y. Kohori, K. Matsuda, and T. Kohara, J. Phys. Soc. Jpn. **65**, 1083 (1996).

[17] N. Emi, R. Hamabata, D. Nakayama, T. Miki, T. Koyama, K. Ueda, T. Mito, Y. Kohori, Y. Matsumoto, Y. Haga, E. Yamamoto, Z. Fisk, and N. Tsujii, J. Phys. Soc. Jpn. **84**, 063702 (2015).

[18] T. Hattori, H. Sakai, Y. Tokunaga, S. Kambe, T. Matsuda, and Y. Haga, J. Phys. Soc. Jpn. **85**, 073711 (2016).

[19] C. Broholm, H. Lin, P. T. Matthews, T. E. Mason, W. J. L. Buyers, M. F. Collins, A. A. Menovsky, J. A. Mydosh, and J. K. Kjems, Phys. Rev. B **43**, 12809 (1991).

[20] F. Bourdarot, E. Hassinger, S. Raymond, D. Aoki, V. Taufour, L.-P. Regnault, and J. Flouquet, J. Phys. Soc. Jpn. **79**, 064719 (2010).

[21] J. Trinh, E. Brück, T. Siegrist, R. Flint, P. Chandra, P. Coleman, and A. P. Ramirez, Phys. Rev. Lett. **117**, 157201 (2016).

[22] M. Werwiński, J. Rusz, J. A. Mydosh, and P. M. Oppeneer, Phys. Rev. B **90**, 064430 (2014).

[23] P. Chandra, P. Coleman, and R. Flint, Nature (London) **493**, 621 (2013).

[24] P. Chandra, P. Coleman, and R. Flint, Phys. Rev. B **91**, 205103 (2015).

[25] M. Sundermann, M. W. Haverkort, S. Agrestini, A. Al-Zein, M. Moretti Sala, Y. Huang, M. Golden, A. de Visser, P. Thalmeier, L. H. Tjeng, and A. Severing, Proc. Natl. Acad. Sci. U.S.A. **113**, 13989 (2016).

[26] C. Bergemann, S. R. Julian, G. J. McMullan, B. K. Howard, G. G. Lonzarich, P. Lejay, J. P. Brison, and J. Flouquet, Physica B (Amsterdam, Neth.) **230**, 348 (1997).

[27] H. Ohkuni, Y. Inada, Y. Tokiwa, K. Sakurai, R. Settai, T. Honma, Y. Haga, E. Yamamoto, Y. Ōnuki, H. Yamagami, S. Takahashi, and T. Yanagisawa, Philos. Mag. B **79**, 1045 (1999).

[28] H. Shishido, K. Hashimoto, T. Shibauchi, T. Sasaki, H. Oizumi, N. Kobayashi, T. Takamasu, K. Takehana, Y. Imanaka, T. D. Matsuda, Y. Haga, Y. Ōnuki, and Y. Matsuda, Phys. Rev. Lett. **102**, 156403 (2009).

[29] E. Hassinger, G. Knebel, T. D. Matsuda, D. Aoki, V. Taufour, and J. Flouquet, Phys. Rev. Lett. **105**, 216409 (2010).

[30] M. M. Altarawneh, N. Harrison, S. E. Sebastian, L. Balicas, P. H. Tobash, J. D. Thompson, F. Ronning, and E. D. Bauer, Phys. Rev. Lett. **106**, 146403 (2011).

[31] D. Aoki, G. Knebel, I. Sheikin, E. Hassinger, L. Malone, T. D. Matsuda, and J. Flouquet, J. Phys. Soc. Jpn. **81**, 074715 (2012).

[32] G. W. Scheerer, W. Knafo, D. Aoki, M. Nardone, A. Zitouni, J. Béard, J. Billette, J. Barata, C. Jaudet, M. Suleiman, P. Frings, L. Drigo, A. Audouard, T. D. Matsuda, A. Pourret, G. Knebel, and J. Flouquet, Phys. Rev. B **89**, 165107 (2014).

[33] S. Tonegawa, K. Hashimoto, K. Ikada, Y.-H. Lin, H. Shishido, Y. Haga, T. D. Matsuda, E. Yamamoto, Y. Onuki, H. Ikeda, Y. Matsuda, and T. Shibauchi, Phys. Rev. Lett. **109**, 036401 (2012).

[34] S. Tonegawa, K. Hashimoto, K. Ikada, Y. Tsuruhara, Y.-H. Lin, H. Shishido, Y. Haga, T. D. Matsuda, E. Yamamoto, Y. Ōnuki, H. Ikeda, Y. Matsuda, and T. Shibauchi, Phys. Rev. B **88**, 245131 (2013).

[35] A. F. Santander-Syro, M. Klein, F. L. Boariu, A. Nuber, P. Lejay, and F. Reinert, Nat. Phys. **5**, 637 (2009).

[36] R. Yoshida, Y. Nakamura, M. Fukui, Y. Haga, E. Yamamoto, Y. Ōnuki, M. Okawa, S. Shin, M. Hirai, Y. Muraoka, and T. Yokoya, Phys. Rev. B **82**, 205108 (2010).

[37] G. L. Dakovski, Y. Li, S. M. Gilbertson, G. Rodriguez, A. V. Balatsky, J.-X. Zhu, K. Gofryk, E. D. Bauer, P. H. Tobash, A. Taylor, J. L. Sarrao, P. M. Oppeneer, P. S. Riseborough, J. A. Mydosh, and T. Durakiewicz, Phys. Rev. B **84**, 161103(R) (2011).

[38] R. Yoshida, K. Tsubota, T. Ishiga, M. Sunagawa, J. Sonoyama, D. Aoki, J. Flouquet, T. Wakita, Y. Muraoka, and T. Yokoya, Sci. Rep. **3**, 2750 (2013).

[39] J.-Q. Meng, P. M. Oppeneer, J. A. Mydosh, P. S. Riseborough, K. Gofryk, J. J. Joyce, E. D. Bauer, Y. Li, and T. Durakiewicz, Phys. Rev. Lett. **111**, 127002 (2013).

[40] S. Chatterjee, J. Trinckauf, T. Hänke, D. E. Shai, J. W. Harter, T. J. Williams, G. M. Luke, K. M. Shen, and J. Geck, Phys. Rev. Lett. **110**, 186401 (2013).

[41] C. Bareille, F. L. Boariu, H. Schwab, P. Lejay, F. Reinert, and A. F. Santander-Syro, Nat. Commun. **5**, 4326 (2014).

[42] T. Durakiewicz, Philos. Mag. **94**, 3723 (2014).

[43] S. Elgazzar, J. Rusz, M. Amft, P. M. Oppeneer, and J. A. Mydosh, Nat. Mater. **8**, 337 (2009).

[44] P. M. Oppeneer, J. Rusz, S. Elgazzar, M.-T. Suzuki, T. Durakiewicz, and J. A. Mydosh, Phys. Rev. B **82**, 205103 (2010).

[45] H. Ikeda, M.-T. Suzuki, R. Arita, T. Takimoto, T. Shibauchi, and Y. Matsuda, Nat. Phys. **8**, 528 (2012).

[46] M. M. Altarawneh, N. Harrison, G. Li, L. Balicas, P. H. Tobash, F. Ronning, and E. D. Bauer, Phys. Rev. Lett. **108**, 066407 (2012).

[47] D. Shoenberg, *Magnetic Oscillations in Metals* (Cambridge University Press, Cambridge, UK, 1984).

[48] R. J. Higgins and D. H. Lowndes, Waveshape analysis in the de Haas–van Alphen effect, in *Electrons at the Fermi Surface*, edited by M. Springford (Cambridge University Press, Cambridge, UK, 1980), Chap. 10, p. 393.

[49] C. Bergemann, A. P. Mackenzie, S. R. Julian, D. Forsythe, and E. Ohmichi, Adv. Phys. **52**, 639 (2003).

[50] J. Wosnitza, V. M. Gvozdikov, J. Hagel, O. Ignatchik, B. Bergk, P. J. Meeson, J. A. Schlueter, H. Davis, R. W. Winter, and G. L. Gard, New J. Phys. **10**, 083032 (2008).

[51] B. J. Ramshaw, B. Vignolle, J. Day, R. Liang, W. N. Hardy, C. Proust, and D. A. Bonn, Nat. Phys. **7**, 234 (2010).

[52] R. Settai, T. Ebihara, M. Takashita, H. Sugawara, N. Kimura, K. Motoki, Y. Onuki, S. Uji, and H. Aoki, J. Magn. Magn. Mater. **140–144**, 1153 (1995).

[53] J. P. Brison, N. Keller, A. Vernière, P. Lejay, L. Schmidt, A. Buzdin, J. Flouquet, S. Julian, and G. Lonzarich, Physica C (Amsterdam, Neth.) **250**, 128 (1995).

[54] A. M. Clogston, Phys. Rev. Lett. **9**, 266 (1962).

[55] H. Harima, K. Miyake, and J. Flouquet, J. Phys. Soc. Jpn. **79**, 033705 (2010).

[56] H. Harima (private communication).

[57] D. Aoki, F. Bourdarot, E. Hassinger, G. Knebel, A. Miyake, S. Raymond, V. Taufour, and J. Flouquet, J. Phys.: Condens. Matter **22**, 164205 (2010).

[58] R. Baumbach, Z. Fisk, F. Ronning, R. Movshovich, J. Thompson, and E. Bauer, Philos. Mag. B **94**, 3663 (2014).

[59] T. D. Matsuda, E. Hassinger, D. Aoki, V. Taufour, G. Knebel, N. Tateiwa, E. Yamamoto, Y. Haga, Y. Ōnuki, Z. Fisk, and J. Flouquet, J. Phys. Soc. Jpn. **80**, 114710 (2011).

[60] T. D. Matsuda, D. Aoki, S. Ikeda, E. Yamamoto, Y. Haga, H. Ohkuni, R. Settai, and Y. Ōnuki, J. Phys. Soc. Jpn. **77**, 362 (2008).

[61] R. Okazaki, Y. Kasahara, H. Shishido, M. Konczykowski, K. Behnia, Y. Haga, T. D. Matsuda, Y. Ōnuki, T. Shibauchi, and Y. Matsuda, Phys. Rev. Lett. **100**, 037004 (2008).

[62] N. R. Werthamer, E. Helfand, and P. C. Hohenberg, Phys. Rev. **147**, 295 (1966).

[63] H. Kusunose, J. Phys. Soc. Jpn. **81**, 023704 (2012).

[64] R. C. Morris, R. V. Coleman, and R. Bhandari, Phys. Rev. B **5**, 895 (1972).

[65] J. M. van Ruitenbeek, W. A. Verhoef, P. G. Mattocks, A. E. Dixon, A. P. J. van Deursen, and A. R. de Vroomen, J. Phys. F: Met. Phys. **12**, 2919 (1982).

[66] J. Spałek, Physica B (Amsterdam, Neth.) **378–380**, 654 (2006).

[67] J. Kaczmarczyk and J. Spałek, Phys. Rev. B **79**, 214519 (2009).

[68] I. Sheikin, A. Gröger, S. Raymond, D. Jaccard, D. Aoki, H. Harima, and J. Flouquet, Phys. Rev. B **67**, 094420 (2003).

[69] A. McCollam, S. R. Julian, P. M. C. Rourke, D. Aoki, and J. Flouquet, Phys. Rev. Lett. **94**, 186401 (2005).

[70] N. Harrison, B. J. Ramshaw, and A. Shekhter, Sci. Rep. **5**, 10914 (2015).

[71] P. Korbel, J. Spałek, W. Wójcik, and M. Acquarone, Phys. Rev. B **52**, R2213(R) (1995).

[72] Y. Ōnuki and A. Hasegawa, *Fermi Surfaces of Intermetallic Compounds* (Elsevier Science, Amsterdam, Neth., 1995), Chap. 135, pp. 1–103.

[73] L. Malone, T. D. Matusda, A. Antunes, G. Knebel, V. Taufour, D. Aoki, K. Behnia, C. Proust, and J. Flouquet, Phys. Rev. B **83**, 245117 (2011).

[74] A. Pourret, A. Palacio-Morales, S. Krämer, L. Malone, M. Nardone, D. Aoki, G. Knebel, and J. Flouquet, J. Phys. Soc. Jpn. **82**, 034706 (2013).

[75] F. D. Boer, J. Franse, E. Louis, A. Menovsky, J. Mydosh, T. Palstra, U. Rauchschwalbe, W. Schlabitz, F. Steglich, and A. D. Visser, Physica B+C (Amsterdam) **138**, 1 (1986).

[76] K. Sugiyama, M. Nakashima, H. Ohkuni, K. Kindo, Y. Haga, T. Honma, E. Yamamoto, and Y. Ōnuki, J. Phys. Soc. Jpn. **68**, 3394 (1999).

[77] G. W. Scheerer, W. Knafo, D. Aoki, G. Ballon, A. Mari, D. Vignolles, and J. Flouquet, Phys. Rev. B **85**, 094402 (2012).

[78] H. Sakai, Y. Tokunaga, S. Kambe, R. R. Urbano, M.-T. Suzuki, P. L. Kuhns, A. P. Reyes, P. H. Tobash, F. Ronning, E. D. Bauer, and J. D. Thompson, Phys. Rev. Lett. **112**, 236401 (2014).

[79] R. Okazaki, T. Shibauchi, H. J. Shi, Y. Haga, T. D. Matsuda, E. Yamamoto, Y. Onuki, H. Ikeda, and Y. Matsuda, Science **331**, 439 (2011).

[80] C. Tabata, T. Inami, S. Michimura, M. Yokoyama, H. Hidaka, T. Yanagisawa, and H. Amitsuka, Philos. Mag. **94**, 3691 (2014).

[81] H. Amitsuka (private communication).

[82] J. Choi, O. Ivashko, N. Dennler, D. Aoki, K. von Arx, S. Gerber, O. Gutowski, M. H. Fischer, J. Strempfer, M. v. Zimmermann, and J. Chang, Phys. Rev. B **98**, 241113(R) (2018).

[83] R. E. Walstedt, S. Kambe, Y. Tokunaga, and H. Sakai, Phys. Rev. B **93**, 045122 (2016).

[84] S. Tonegawa, S. Kasahara, T. Fukuda, K. Sugimoto, N. Yasuda, Y. Tsuruhara, D. Watanabe, Y. Mizukami, Y. Haga, T. D. Matsuda, E. Yamamoto, Y. Onuki, H. Ikeda, Y. Matsuda, and T. Shibauchi, Nat. Commun. **5**, 4188 (2014).

[85] S. C. Riggs, M. Shapiro, A. V. Maharaj, S. Raghu, E. Bauer, R. Baumbach, P. Giraldo-Gallo, M. Wartenbe, and I. Fisher, Nat. Commun. **6**, 6425 (2015).

[86] P. M. Oppeneer, S. Elgazzar, J. Rusz, Q. Feng, T. Durakiewicz, and J. A. Mydosh, Phys. Rev. B **84**, 241102(R) (2011).

[87] J. Buhot, M.-A. Méasson, Y. Gallais, M. Cazayous, A. Sacuto, G. Lapertot, and D. Aoki, Phys. Rev. Lett. **113**, 266405 (2014).

[88] M. B. Maple, J. W. Chen, Y. Dalichaouch, T. Kohara, C. Rossel, M. S. Torikachvili, M. W. McElfresh, and J. D. Thompson, Phys. Rev. Lett. **56**, 185 (1986).

[89] A. R. Schmidt, M. H. Hamidian, P. Wahl, F. Meier, A. V. Balatsky, J. D. Garrett, T. J. Williams, G. M. Luke, and J. C. Davis, Nature (London) **465**, 570 (2010).

[90] P. Aynajian, E. H. da Silva Neto, C. V. Parker, Y. Huang, A. Pasupathy, J. Mydosh, and A. Yazdani, Proc. Nat. Acad. Sci. U.S.A. **107**, 10383 (2010).

[91] P. Chandra, P. Coleman, R. Flint, J. Trinh, and A. Ramirez, Physica B (Amsterdam, Neth.) **536**, 145 (2018).

[92] G. Amoretti, J. Phys. France **45**, 1067 (1984).

[93] F. J. Ohkawa and H. Shimizu, J. Phys.: Condens. Matter **11**, L519 (1999).

[94] J. Sichelschmidt, V. A. Ivanshin, J. Ferstl, C. Geibel, and F. Steglich, Phys. Rev. Lett. **91**, 156401 (2003).

[95] C. Krellner, T. Förster, H. Jeevan, C. Geibel, and J. Sichelschmidt, Phys. Rev. Lett. **100**, 066401 (2008).

[96] B. I. Kochelaev, S. I. Belov, A. M. Skvortsova, A. S. Kutuzov, J. Sichelschmidt, J. Wykhoff, C. Geibel, and F. Steglich, Eur. Phys. J. B **72**, 485 (2009).

[97] P. Wölfle and E. Abrahams, Phys. Rev. B **80**, 235112 (2009).

[98] P. Schlottmann, Phys. Rev. B **79**, 045104 (2009).

[99] D. L. Randles, Proc. R. Soc. London, Ser. A **331**, 85 (1972).
[100] H. Aoki, N. Kimura, and T. Terashima, J. Phys. Soc. Jpn. **83**, 072001 (2014).
[101] V. P. Mineev, arXiv:1504.05020.
[102] S. A. Brazovskii and I. A. Luk'yanchuk, Zh. Eksp. Teor. Fiz. **96**, 2088 (1989) [Sov. Phys. JETP **69**, 1180 (1989)].
[103] R. Ramazashvili, Phys. Rev. Lett. **101**, 137202 (2008).
[104] R. Ramazashvili, Phys. Rev. B **79**, 184432 (2009).
[105] E. Langmann, Phys. Rev. B **46**, 9104 (1992).
[106] T. Kita and M. Arai, Phys. Rev. B **70**, 224522 (2004).
[107] M. Nakashima, H. Ohkuni, Y. Inada, R. Settai, Y. Haga, E. Yamamoto, and Y. Onuki, J. Phys.: Condens. Matter **15**, S2011 (2003).